Final Report

Project Title Formation of nanorods for sensing: Hydrothermal conversion of nanoparticles films to arrays of nanorods

By

Dr. Sirikanjana Thongmee

June/ 2013

Contract No. MRG5480254

Final Report

Project Title: Formation of nanorods for sensing: Hydrothermal conversion of nanoparticles films to arrays of nanorods

Researcher	Institute
1. Dr. Sirikanjana Thongmee	Kasetsart University
2. Prof. Dr. I Ming Tang	Mahidol University
3. Prof. Dr. Jun Ding	National University of Singapore

This project granted by the Thailand Research Fund and Kasetsart University

Abstract

Project Code : MRG5480254

Project Title : Formation of nanorods for sensing: Hydrothermal conversion of nanoparticles films to arrays of nanorods

Investigator : 1. Prof. Dr. I Ming Tang

2. Prof. Dr. Jun Ding

E-mail Address : fscisjn@ku.ac.th

Project Period : 2 years

Abstract:

ซิงค์ออกไซด์และอะลูมิเนียมเจือซิงค์ออกไซด์สังเคราะห์โดยใช้เทคนิคไฮโดรเทอร์ลมอล การเจืออะลูมิเนียมโดยใช้ความเข้มข้นที่แตกต่างกันทำให้โครงสร้างของซิงค์ออกไซด์เปลี่ยนไป ผลจาก XRD แสดงให้เห็นว่า สารตัวอย่างที่ได้มีโครงสร้างแบบเฮกสะโกนอลซึ่งเป็นโครงสร้างของซิงค์ออกไซด์และไม่พบเฟสของอะลูมิเนียมและสารเจือปนอื่นที่เจือลงไปในซิงค์ออกไซด์เลย ค่าแลตทิชของ a และ c ของซิงค์ออกไซด์ที่คำนวณได้จากการทดลองมีค่าดังนี้ a = 3.249 nm และ c = 5.207 nm ตามลำดับ ผลจาก SEM พบว่า เส้นผ่านศูนย์กลางของซิงค์ออกไซด์มีค่า 200 - 300 nm และความยาวของซิงค์ออกไซด์มีค่า 1-2 μm แต่เมื่อเจืออะลูมิเนียมลงไปในซิงค์ออกไซด์ทำให้โครงสร้างของซิงค์ออกไซด์เปลี่ยนไปโดยที่นาโนรอดจะมีขนาดเล็กและสั้นลง ส่วนผลของรามานนั้นแสดงให้เห็นว่า จะพบพีคที่เด่นชัดที่ตำแหน่ง 437 cm^{-1} ซึ่งสัมพันธ์กันกับ E2(high) โหมด แสดงให้เห็นถึงโครงสร้างของซิงค์ออกไซด์ นอกจากนี้ยังพบพีคที่กว้างที่ตำแหน่ง 575 cm^{-1} ด้วย ส่วนผลของ PL จะแสดงพีคที่กว้างที่ตำแหน่ง 575 nm ซึ่งเป็นการแทนที่ของออกซิเจนและอีกพีคหนึ่งซึ่งมีลักษะแคบและคมชัดนั้นจะอยู่ที่ตำแหน่ง 380 nm ซึ่งอยู่ใกล้ขอบการดูดกลืนของเอกซิตอน เมื่ออะลูมิเนียมเจือเข้าไปในซิงค์ออกไซด์จะพบพีคที่ตำแหน่ง 574 nm ซึ่งเป็นการดูดกลืนในช่วงแสงสีเหลือง

Undoped and aluminum doped zincoxide (ZnO) have been synthesized by using sodium hydroxide (NaOH) assisted hydrothermal technique. By doping and varying Al concentrations, the morphology of the Al doped ZnO nanostructures can be readily changed. The XRD patterns reveal well-developed reflections of hexagonal wurtzite ZnO without any indications of the phases related with Al or other impurities such as Al_2O_3, $ZnAl_2O_4$, NaOH etc. The lattice parameters a and c were 3.249 nm and 5.207 nm, respectively. The morphologies of the undoped and Al-doped ZnO nanorods were characterized by scanning electron microscopy (SEM). The results showed the morphology of pure ZnO nanorods with diameter of 200 - 300 nm and the lengths of 1-2 μm. When Al was doped into ZnO the morphologies of nanorods were changed a little bit by nanorods became shorter and smaller. The Raman results indicated the sharp peak located at 437 cm^{-1} corresponding to E2(high) mode indicates the typical wurtzite structure of ZnO and good crystallization and the broad peak centered at 575 cm^{-1} assigned to A1(LO) mode is also detected. The PL results showed that the broad emission band around 575 nm can be attributed to the interstitial oxygen ions and the one is the UV emission at 380 nm, which is the near-band edge exciton related emission and other is the deep level emission. The Al doped ZnO nanorods exhibits a yellow emission peak at 574 nm. The strong UV emission, which strongly relate to crystallite quality of ZnO, is contribute by conduction valence band combination (∼ 375 nm). It is shallow donor (∼ 395 nm) and Zn interstitial (∼ 420 nm)

Keywords : ZnO nanorods, Al doped ZnO, hydrothermal, gas sensor

Executive summary

Nowadays, the detection of toxic and flammable gases such as NO2, CO, NH3, H2, H2S, CH4, etc. in the environment is of paramount importance for personal health and public security; especially in the automotive, aerospace, semiconductor, utility, and power industries. For such detection, chemical sensors are among the most useful owing to their reliability, life expectancy, and low cost. At the same time, metal oxides have remarkable properties, such as high sensitivity to changes in a chemical environment. With the appropriate doping, structure processing, and operating temperature, they can be manufactured into commercial sensors.

The operating principle of metal-oxide (ZnO, SnO2, TiO2, and In2O3) devices is based on the transduction of adsorbed chemicals on the sensor surface with a corresponding change in the electrical conductance. The challenge is to build sensors not only with enhanced sensitivity, but also with the ability to detect specific chemicals in a complex environment (selectivity), and to be quickly reset for the next sensing cycle (refresh ability). With the advent of nanotechnology, nanostructured materials with novel characteristics seem set to address these challenges.

Quasi-one-dimensional (Q1D) metal oxides nanostructures (nanowires, nanobelts, and nanotubes) have several advantages with respect to their traditional thin-and thick films counterpart such as very large surface-to-volume ratio, dimensions comparable to the extension of surface charge

region, superior stability owing to the high crystallinity, modulation of their operating temperature to select the proper gas semiconductor reactions, catalyst deposition over the surface for promotion or inhibition of specific reactions, and the possibility of field-effect transistors (FET) configuration that allows the use of gate potential to customize sensitivity and selectivity.

There are several techniques used to prepare metal oxide nanowires such as vapour phase transport, chemical vapour deposition, chemical deposition, electrical deposition, and template growth.

In this project, nanoparticle films of ZnO are converted into arrays of nanorods by the hydrothermal method which is a low temperature aqueous synthesis technique. The hydrothermal method involves heating the nanoparticles to 90 $^{\circ}$C for twenty four hours at some appropriate pH. This method has aroused much interest since it involves low cost and is especially favorable to the environmental. Once we have achieved film of aligned nanorods, we will study the functionalized of useful chemical molecules on the surface of the rods. The nanorods are better than the nanoparticles since their surface to volume ratios are greater. This will lead to savings in the amount of chemicals needed. We will be conducting characterization studies on the array of nanorods at the first stages of the investigation. In the second phase we will be concerned with the functionalizing inorganic (Cu and Al) compounds which will interact with CO gas after that we will consider doing prototype. This is because we have to confirm that the results are good enough for making the prototype. Before doing

the prototype we need the close box for applying the mixture of gas to test CO gas from ZnO nanorods doped Cu or Al.

For prototype, a typical infrared (IR) system for sensing gas concentrations in air consists of a thermal grey body radiation emitter, an absorption path, optical elements, and an IR detector. The specific system presented here consists of a micro-machined infrared emitter, an absorption path and a photo-acoustic cell with a build-in microphone and a thermopile (Figure 1, 2 and 3).

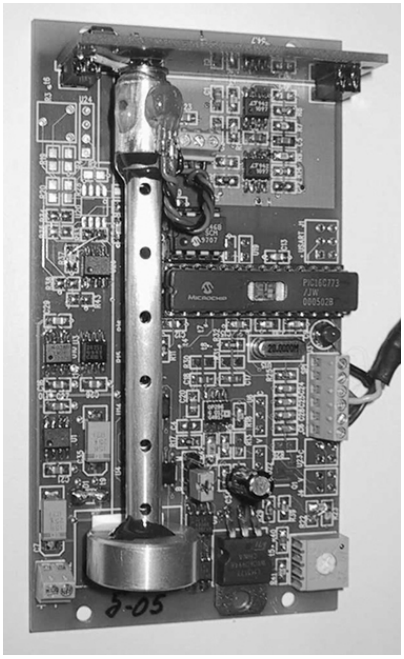

Figure1: Picture of the 54.7 Gas Monitoring Module.

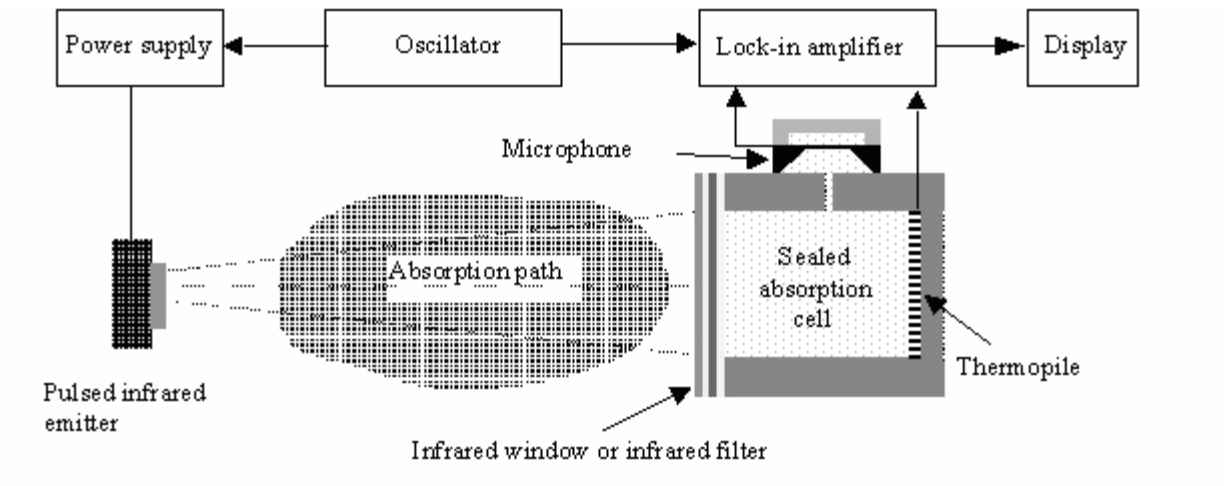

Figure 2: Schematic principle of operation for the 54.7 photoacoustic gas sensing module.

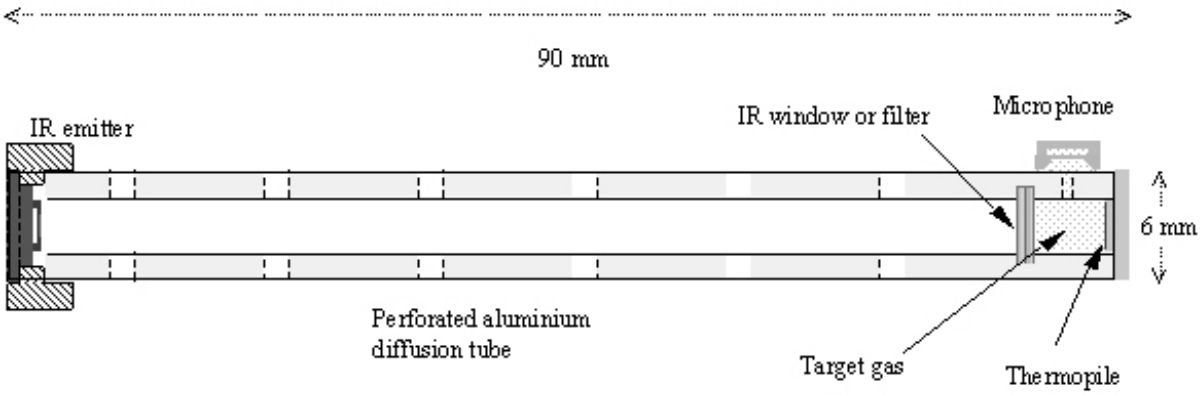

Figure3: The 54.7 photoacoustic gas sensing cell.

The emitter is modulated at a frequency of 20 Hz, emitting infrared light with an approximate grey body spectral distribution. Presence of gas in the absorption path reduces the light intensity at the gas specific absorption wavelengths. Before reaching the photo-acoustic cell, the light is optionally

transmitted through a broadband pass interference filter, designed to let the transmitting band envelop the absorption pattern of the target gas. Transmitted light enters the photo-acoustic cell, which is filled with a target gas, identical to the gas to be detected. Most of the light corresponding to the gas specific absorption wavelengths gets absorbed in the enclosed cavity. This leads to a pressure increase inside the cell, which is measured by the microphone. The gas concentration in the absorption path is related to the pressure decrease in the cell, and is thereby determined. The silicon microphone is manufactured by making use of silicon micromachining and wafer bonding.

Behind the PA-cell the remaining light reaches a thermopile IR detector, enabling continuous calibration of the light intensity emitted by the infrared source. This signal is used to compensate for changes in the measurement path, for instance due to moisture, dirt, or other effects. Optionally, an optical filter is placed in front of this detector, to minimise the effect of target gas absorption on the calibration signal.

Many gases are suitable to be measured using this technique. It has been tested with CO_2, N_2O, CH_4, SF_6, R_{404a} and R_{134a}. We have been able to measure down to 10 ppm N_2O, 2 ppm CO_2, 50 ppm CH_4, 1 ppm R_{134a} and 5 ppm SF_6. Many other gases are suitable to be monitored by this technique and an appreciable potential sensitivity enhancement remains to be exploited.

Objective

1. To fabricate ZnO nanorods by using hydrothermal method

2. To study the properties of the array of nanorods by using X-Ray diffraction (XRD), Scanning Electron Microscopy (SEM), Raman spectroscopy, and Photoluminescence (PL)

3. To functionalize the surface of the nanorods with inorganic (Cu and Al) compounds this would interact with CO gas.

4. To test the ZnO nanorods with doping Cu or Al for catching the CO gas then, starting to make the prototype.

Research methodology

Pure ZnO and Al-doped ZnO nanorods were grown on Si substrate by using seed-assisted hydrothermal method. The Si substrate (100) was cleaned using ultrasonic cleaning methods and rinsed in acetone for 15 min to remove pollutants from the surface of silicon substrate. The seed layer of ZnO films (100 nm) were first grown by RF magnetron puttering and in-situ annealing at 300 ^{O}C for 1 hour. In a typical synthesis process, the substrate with ZnO seed layer was placed in an aqueous solution of 0.025M zinc nitrate hexahydrate ($Zn(NO_3)_2 \cdot 6H_2O$) appropriate amount of Aluminum nitrate $Al(NO_3)_3$ were dissolved by deionized water and 60 ml solution was received, and 60 ml of sodium hydroxide

(NaOH) (5.0 mol/l) aqueous solution was slowly dripped into the former solution under magnetic stirring. Subsequently, the mixture was transferred into a 200 ml Teflon lined autoclave. Then the autoclave was sealed and maintained at 150 ˚C for 20 hours. After the reaction is complete, the precipitate is collected, washed with deionized water in the final products and finally dried at 100 ˚C for 5 hours.

The crystalline structure of the Al-doped ZnO samples was determined by X-ray diffraction (Cu K_α radiation, λ = 0.154056 nm). The morphology of as prepared un-doped and Al- doped ZnO sample were investigated by scanning electron microscopy (SEM). The optical property was characterized by Raman spectroscopy and Photoluminescence (PL).

Then, the ZnO nanorod samples will be testing the gas by putting in the closed box for applying CO gas to test the resistance response during cyclic exposure with the increasing concentrations of CO gas in dry air at various operating temperatures.

Result and Discussion

The X-ray diffraction (XRD) was used to study the structure of ZnO nanorods. Figure 1 shows the X-ray diffraction patterns of the samples, which are prepared with the different Al-doped ZnO nanorods. The effects of different aluminum doped ZnO on the crystallographic structure are not revealed in Fig. 1. The XRD patterns reveal well-developed reflections of hexagonal wurtzite ZnO

(JCPDS card No.036-1451), without any indications of the phases related with Al or other impurities such as Al_2O_3, $ZnAl_2O_4$, NaOH etc. The lattice parameters a and c are 3.249 nm and 5.207 nm, respectively. This finding implies that the aluminum doping most probably occurs by substituting zinc atoms in the crystal structure. In comparison with the undoped sample by the increase in the intensity of ZnO peaks. The most intensive peak presented is shown as (101) plane and additional peaks along with (100) and (002) planes are also observed. The improvement of the crystallinity of ZnO nanorods with increasing Al-doping contents is ascribed to the surface diffusion of the increasing adsorbed atoms, inducing an improvement of the quality and crystallinity. Although the absolute intensities of the peaks increased with the increasing of aluminum concentration, the intensities of these lines almost remained constant upon Al doping.

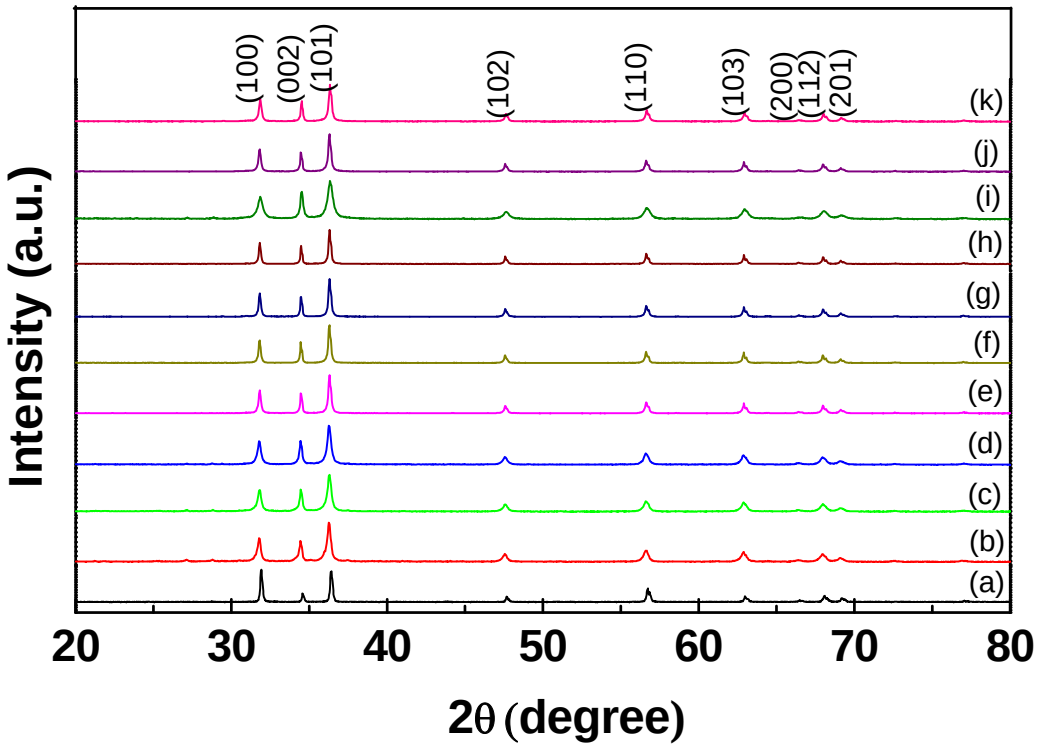

Figure 1: X-ray diffraction patterns of Al-doped ZnO nanorods: (a) ZnO, (b) 1at%Al, (c) 2at%Al, (d) 3at%Al, (e) 4at%Al, (f) 5at%Al, (g) 6at%Al, (h) 7at%Al, (i) 8at%Al, (j) 9at%Alm and (k) 10at%Al.

The morphologies of the undoped and Al-doped ZnO nanorods were characterized by scanning electron microscopy (SEM). Figure 2 shows SEM images of Al-doped ZnO nanorods. It was found that the morphology of pure ZnO nanorods with diameter of 200 - 300 nm and the lengths of 1-2 μm. When Al was doped into ZnO the morphologies of nanorods were changed a little bit by nanorods became shorter and smaller (Fig. 2(b)). The diameter of nanorods was 80-100 nm. When concentration of Al more than 3at% the ZnO nanorods was irregular-shape particle as shown in Fig. 2(c) – 2(f)), which

implied that a higher Al-doping concentration had the effect on the ZnO growth. However, the exact mechanism about the influence of Al ions on the ZnO growth has not been understood and intensive studies should be done in the future.

The chemical compositions of the as-prepared nanorods were analyzed by energy-dispersive X-ray spectroscopy (EDX). The corresponding EDX spectra of Al-doped ZnO nanorods taken in the SEM mode are shown in Fig. 3. For pure ZnO nanorods, besides the lines of the constitutive elements Zn and O, the EDX spectrum gave no indication for the other elements, confirming the phase-purity of the sample as shown the Fig. 3(a). The EDX spectra performed on the Al-doped ZnO nanorods confirmed the simultaneous presence of Zn, O, and Al was shown in Fig. 3(b)-3(f). EDX measurements on different sports of the samples always give the same pattern, which prove the good homogeneity of the samples.

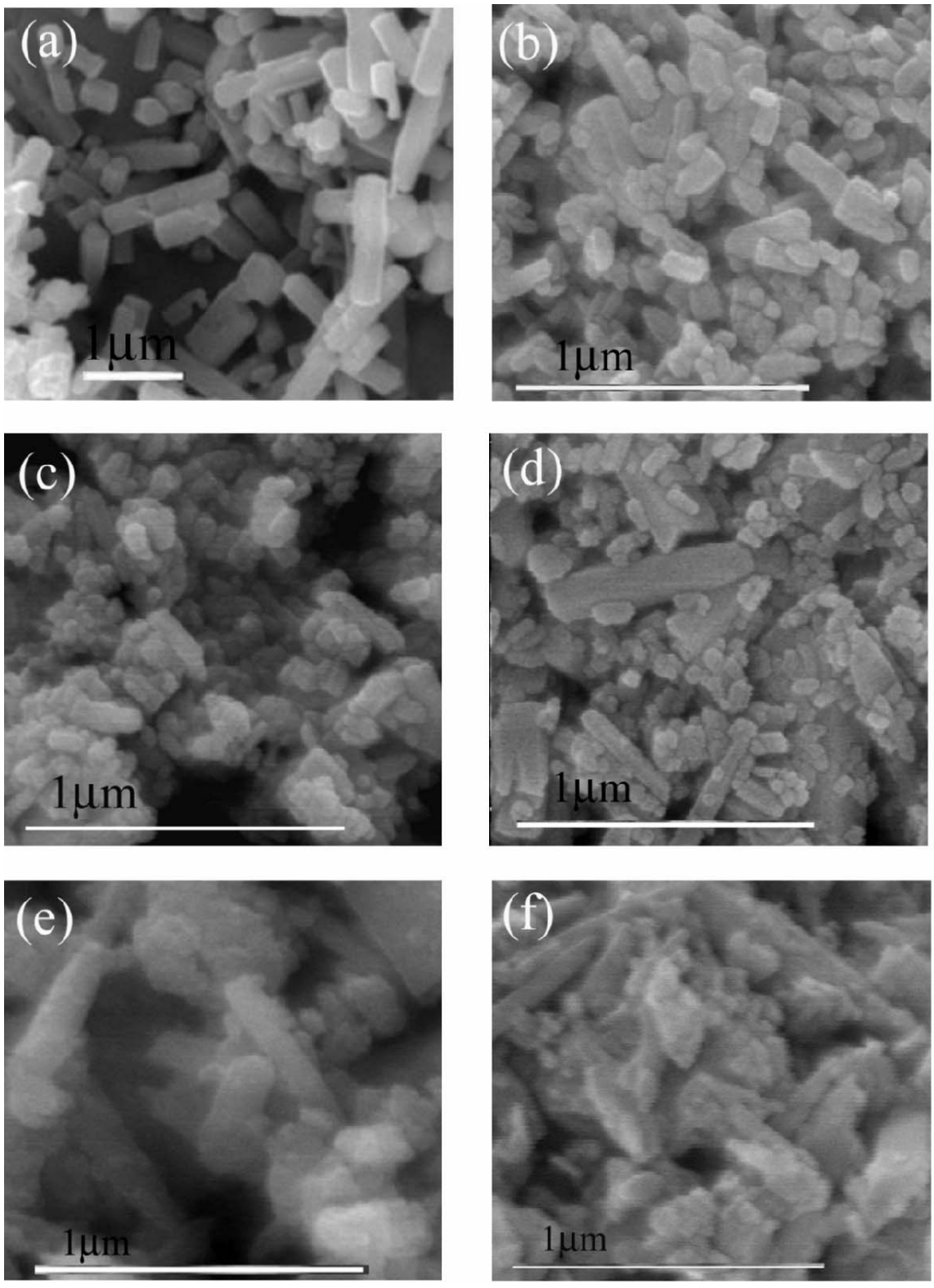

Figure 2: shows SEM images of Al-doped ZnO nanorods: (a) ZnO, (b) 1at%Al, (c) 3at% Al, (d) 5at% Al, (e) 7at%Al, and (f) 10at%Al.

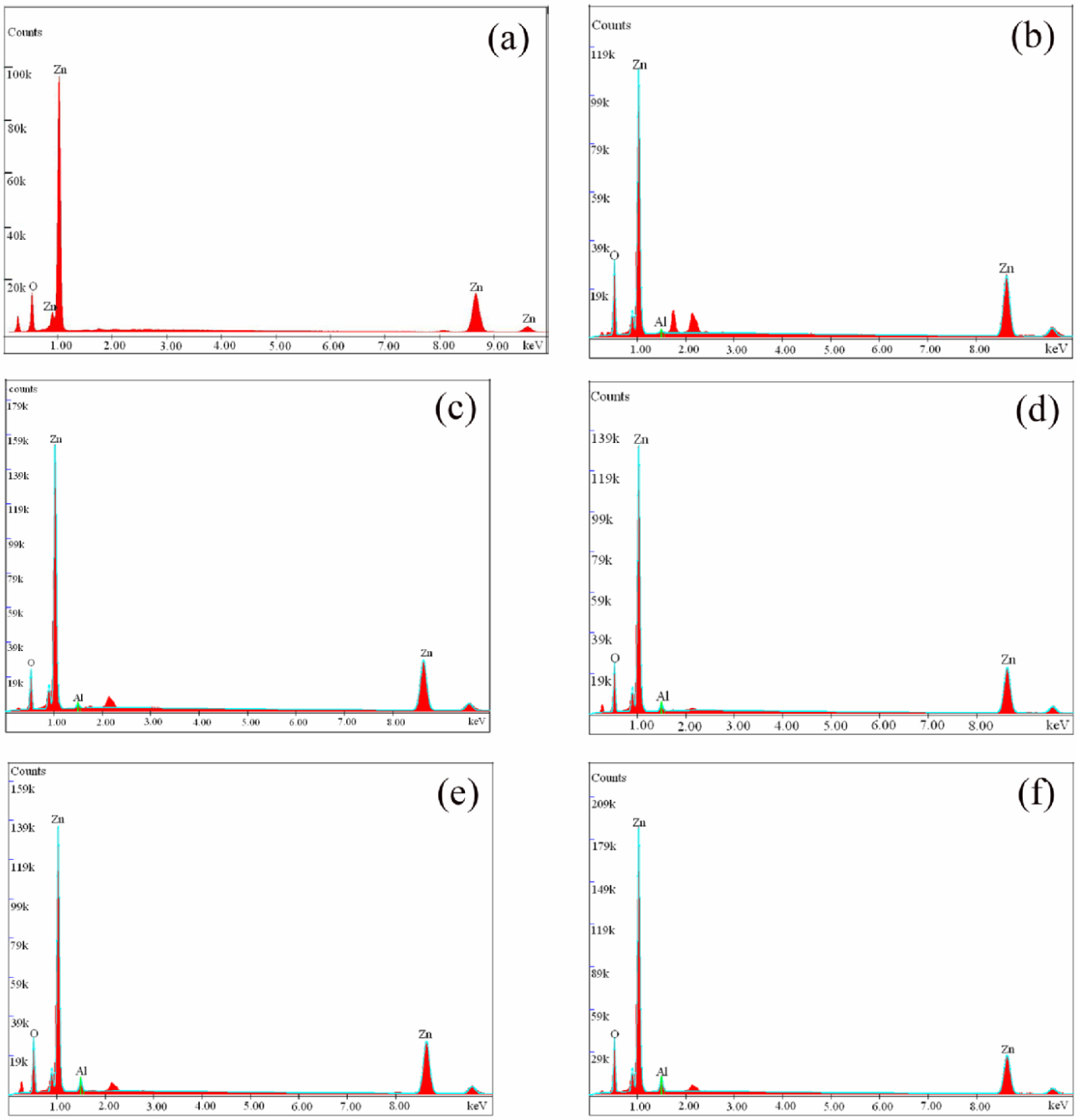

Figure 3: EDX spectra of ZnO nanorods: (a) ZnO, (b) 1at%Al, (c) 3at%Al, (d) 5at%Al; (e) 7at%Al, and 10at%Al.

The Raman-scattering spectra of the as grown ZnO structures are shown in Figure 4 with 514 nm laser green light as an excitation source. The Raman signals are usually very sensitive to the structure of crystal as well as to the defects in the crystal structure. The crystal structure of ZnO is wurtzite (hexagonal) which belongs to the C_{6v} symmetry group and gives the Raman-active optical phonon modes classified as A_1+ E_1+ $2E_2$ [1]. In addition, A1 and E1 modes are polar and split into transverse optical (TO) and longitudinal optical (LO) phonons. As a wide band gap oxides semiconductor, it is well known that ZnO has a strong optical absorption to the ultraviolet light (UV, e.g. 325 nm) and transparency to the visible light (e.g. 532 nm). Therefore, the UV Raman spectroscopy is more sensitive to the surface region of the sample, whereas the visible Raman spectroscopy gives not only the information of the surface but also the inner information of the sample [2].

Figure 4 gives the Raman spectra of the pure ZnO and Al doped ZnO nanostructures. The sharp peak located at 437 cm^{-1} corresponding to E2(high) mode indicates the typical wurtzite structure of ZnO and good crystallization. A transverse optical (TO) phonon mode was detected at 377 cm^{-1} (A1). The peaks at 328, 548, 724, 1052, 1065 and 1384 cm^{-1} are known to be multi-phonon responses [3-5]. In addition, the broad peak centered at 575 cm^{-1} assigned to A1(LO) mode is also detected. However, these spectra clearly indicate that all the samples exhibit the well-known characteristics of the wurtzite structure of ZnO crystal. Therefore, the enhancement of surface-related phonon mode might be resulted

from the doping of Al ions and/or the different morphology of ZnO nanostructures. The Al ions in ZnO host and different morphology of ZnO may change the electromagnetic interaction at the interfaces between the nanostructures.

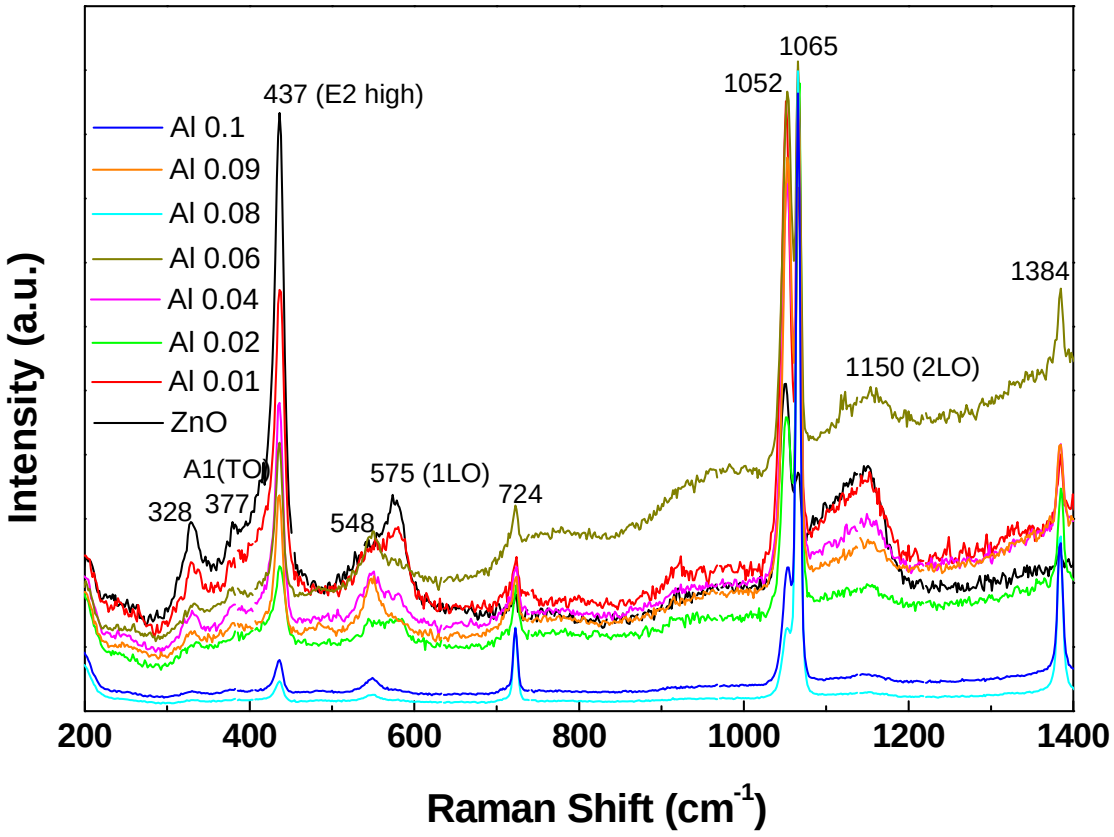

Figure 4: Room temperature Raman spectra of pure ZnO and Al doped ZnO nanorods. All the samples show qualitatively identical Raman shifts and they match well with the spectrum for wurtzite ZnO crystal.

The photoluminescence measurement of ZnO nanorods were performed with an excitation wavelength 325 nm at room temperature. Figure 5 shows the PL spectra of ZnO nanorods at room temperature growth by hydrothermal technique with various Al doping concentrations. The PL spectra showed that the ZnO nanorods have two clear emission bands. For the two clear emission bands, one is a relatively weak and narrow UV emission centered about 380 nm that is widely accepted due to the exciton emission from conduction band to valence band and the other is much stronger and broader emission observed in the yellow range of visible spectrum with an emission peak around 574 nm that is believed to be caused by extrinsic impurities such as absorbed water or surface hydroxyl groups. The strong UV emission, which strongly relate to crystallite quality of ZnO, is contribute by conduction valence band combination (∼ 375 nm). It is shallow donor (∼ 395 nm) and Zn interstitial (∼ 420 nm) [6-8].

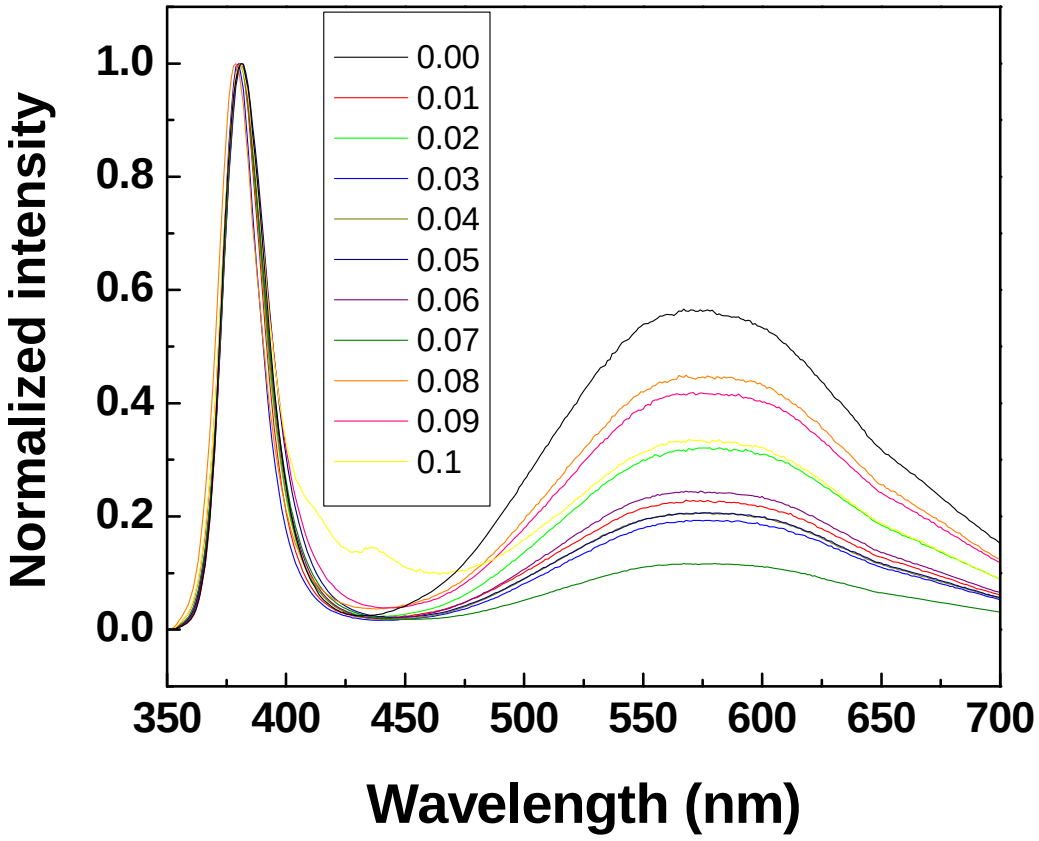

Figure 5: PL spectra of pure ZnO and AL doped ZnO nanorods using 325 nm line as the exciting source.

The relative response (S) to a target gas is defined as the ratio of the change in conductance of a sample upon exposure of the gas to the original conductance in air. The relation for S is given as

$$S = \frac{G_g - G_a}{G_a}$$

where Ga is the conductance in air and Gg the conductance in a sample gas.

Specificity or selectivity is defined as the ability of a sensor to respond to a certain gas in the presence of different gases. Response time (RST) is defined as the time needed for a sensor to attain 90% of the maximum increase in conductance on exposure to the target gas. Recovery time (RCT) is the time taken to get back 90% of the original conductance in air.

We fabricated Al-doped ZnO nanorods gas sensor as a function of Al doping concentrations of 0 – 6% on sapphire substrate to form two Au top electrodes, to investigate the Al-doping effect on the sensitivity of Al-doped ZnO nanorods gas sensor for ethanol gas and CO gas. Response is calculated from dynamics response according to:

$$\text{Response} = \frac{R_a}{R_g}$$

Where R_a = resistance in air and R_g = resistance in reducing gas such as ethanol and CO.

In this work, we have tested the gas at two temperatures. There are 300 $^{\circ}$C and 350°C for ethanol. The result of testing ethanol is shown in Figure 6.

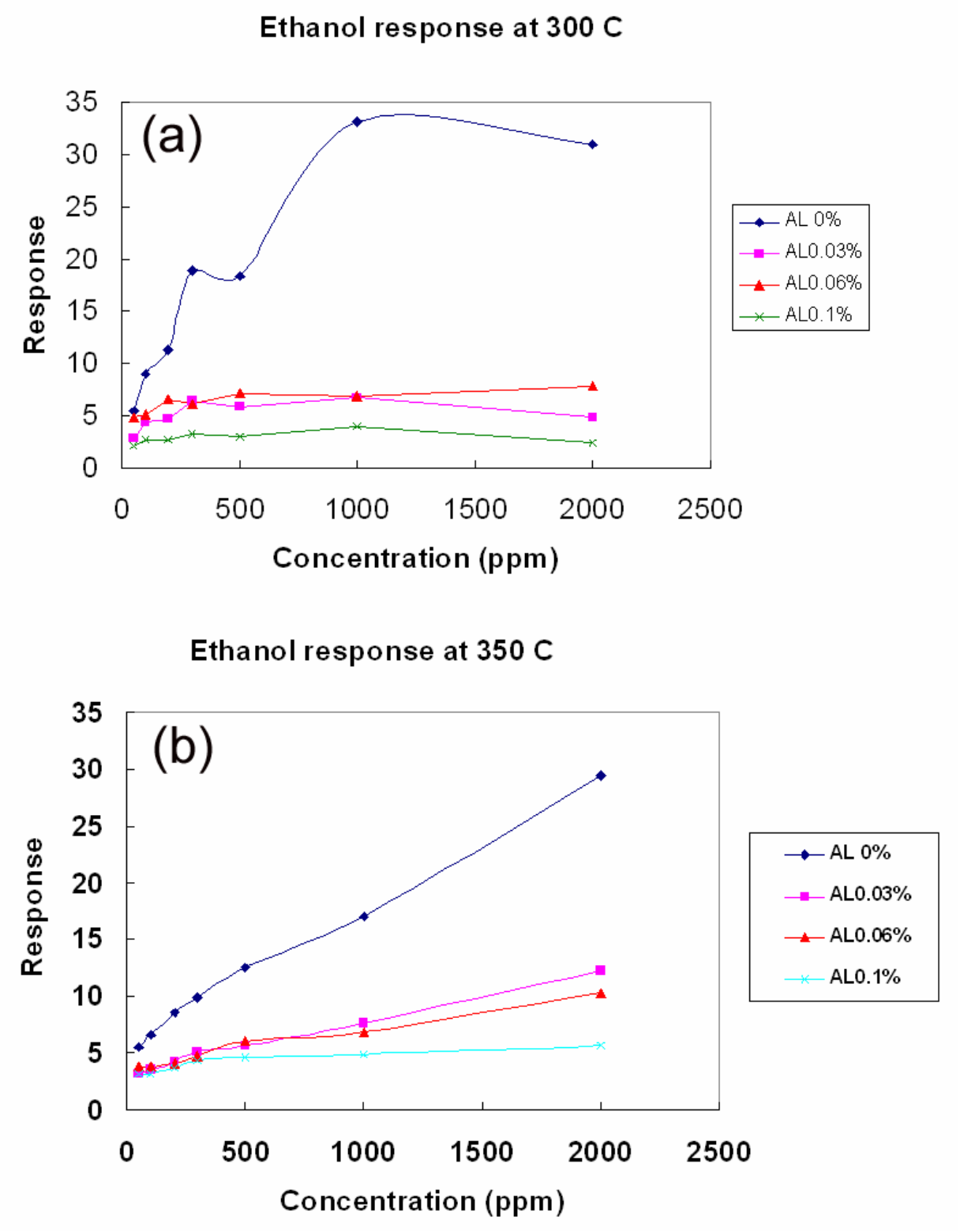

Figure 6: Response of pure ZnO and different concentration of Al doped ZnO nanorods gas sensor with an increase in ethanol concentration: (a) at temperature 300 $^{\circ}$C and (b) at temperature 350°C.

Figure 6(a) shows the response of pure ZnO and Al doped ZnO nanorods for various ethanol concentrations at 300 $^{\circ}$C. The results indicates that pure ZnO turn intoan almost conductive surface from insulating it and even inside ZnO nanorods over ethanol concentration of around 1100 ppm. At the higher concentration of ethanol (> 1200 ppm), the response seems to be decreased. For Al doped ZnO nanorods, the response does not change. This may be due to the Al doped into ZnO nanorods donot affect to the ethanol at temperature 300 $^{\circ}$C. When the temperature is turned to be 350°C, the response increased with increasing the concentration of ethanol for all the samples as shown in Figure 6(b). However, the pure ZnO nanorods still shows a good result more than Al doped ZnO nanorods. The responses of Al doped ZnO nanorods slightly increased but the results are not evident compare to pure ZnO nanorods. This may be due to the changing of structure of ZnO nanorods at higher concentration of Al doping.

For CO gas testing, we only tested at 300 $^{\circ}$C because of very low response in ethanol gas. From the graph, CO response of pure ZnO and Al doped ZnO nanorods tend to decrease with the increasing of CO concentration. The response is slightly more than 1.

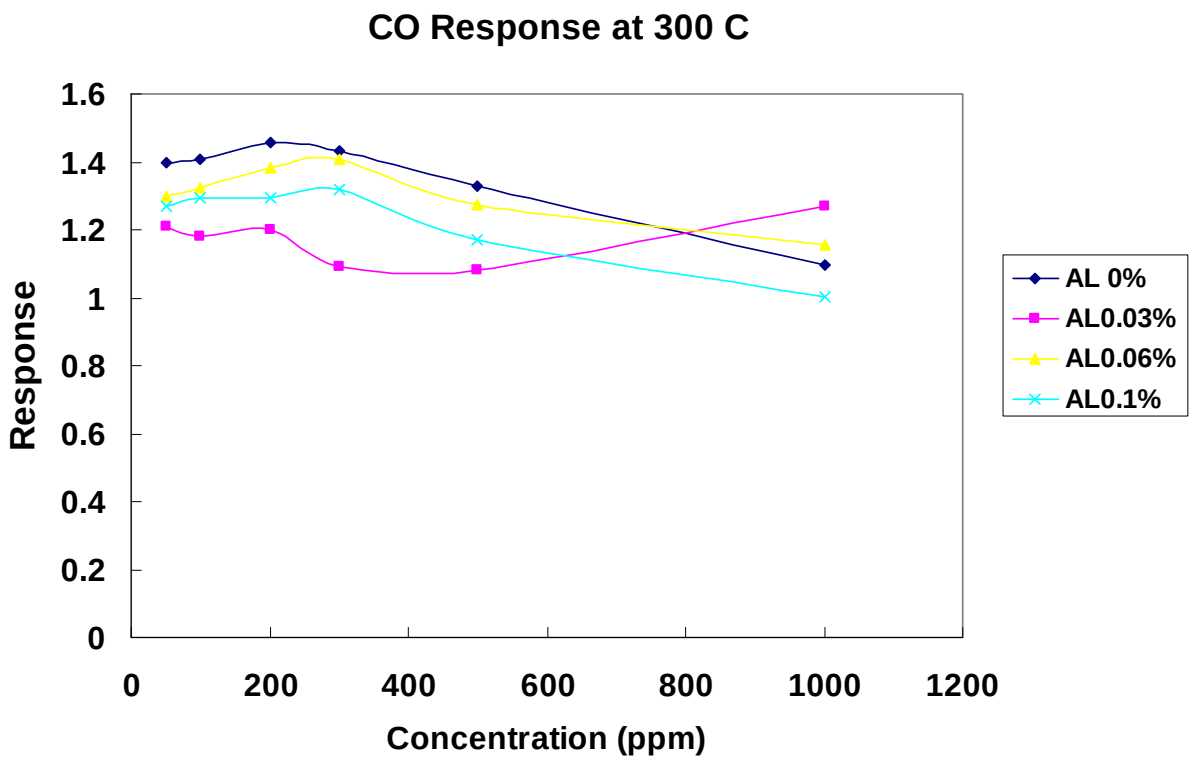

Figure 7: The response of pure ZnO and Al doped ZnO nanorods at various concentration of CO gas at 300 $^{\circ}$C.

Conclusion

In conclusion, Al-doped zinc oxide nanorods were successfully grown on a silicon substrate using a hydrothermal process. The effect of Al doping on the elemental composition, microstructure characteristics and optical properties of the nanorod arrays has been studied. XRD patterns illustrate that the nanorods were ZnO wurtzite structure. The Raman results indicated the sharp peak located at 437 cm^{-1} corresponding to E2(high) mode indicates the typical wurtzite structure of ZnO and good

crystallization and the broad peak centered at 575 cm^{-1} assigned to A1(LO) mode is also detected. The PL spectra showed that the ZnO nanorods have two clear emission bands. For the two clear emission bands, one is a relatively weak and narrow UV emission centered about 380 nm that is widely accepted due to the exciton emission from conduction band to valence band and the other is much stronger and broader emission observed in the yellow range of visible spectrum with an emission peak around 574 nm that is believed to be caused by extrinsic impurities such as absorbed water or surface hydroxyl groups.

References

[1] Y. Tong, Y. Liu, C. Shao, Y. Liu, C. Xu, J. Zhang, Y. Lu, D. Shen, X. Fan, J. Phys. Chem. B **110** (2006) 14714.

[2] M. Li, Z. Feng, G. Xiong, P. Ying, Qin Xin, Can Li, J. Phys. Chem. B **105** (2001) 8107.

[3] T. C. Damen, S. P. S. Porto and B. Tell, Phys. Rev. **142** (1966) 570 .

[4] C. Bundesmann, N. Ashkenov, M. Schubert, D. Spemann, T. Butz, E. M. Kaidashev, M. Lorenz and M Grundmann, Appl. Phys. Lett. **83** (2003) 1074.

[5] W. Gebicki, K. Osuch, C. Jastrezebski, Z. Golacki and M. Godlewski, Superlattices Microstruct. **38**, (2005) 428.

[6] M.W. Ahn, K.S. Park, J.H. Heo, J.G. Park, D.W. Kim, K.J. Choi, J.H. Lee, S.H. Hong, Applied Physics Letters **93**, (2008) 263103(1) - 263103(3).

[7] L.M. Li, Z.F. Du, T.H. Wang, Sensors and Actuators B: Chemical **147** (2010) 165.

[8] N. Han, X. Wu, L. Chai, H. Liu, Y. Chen, Sensors andActuators B: Chemical **150** (2010) 230.

Appendix

Hydrothermal synthesis and optical properties of Al doped ZnO nanorods

S. Thongmee[1,2] B. Sukluan[1], G.S. Chen[3], T.S. Herng[4], J. Ding[4] W. Samanjit[5],

V. Krongtong[5], and I.M. Tang[2]

[1]Department of Physics, Faculty of Science, Kasetsart University

Bangkok 10900, Thailand.

[2]Department of Materials Science, Faculty of Science, Kasetsart University

Bangkok 10900, Thailand.

[3]Department of Physics, Faculty of Science, National University of Singapore,

Singapore 117551.

[4]Department of Materials Science and Engineering, Faculty of Engineering,

National University of Singapore, Singapore 117576.

[5]National Metal and Materials Technology Center, Phahonyothin Road,

Khlong Nueng, Khlong Luang, Pathum Thani 12120, Thailand

Keywords: ZnO nanorods, hydrothermal method, Al doped ZnO, hexagonal wurtzite structure

Corresponding author: fscisjn@ku.ac.th ;

Tel: (+66) 2 562 5555 ext 3017,

Fax: (+66) 2 942 8029

Abstract

Zinc oxide nanorods with different Al doping contents were prepared by the hydrothermal technique. The effects of Al doping on the structural characteristics and optical properties of the nanorods were studied. The morphology and microstructure of as-synthesized samples were characterized by X-ray diffraction (XRD) spectra, scanning electron microscopy (SEM), Raman spectroscopy and Photoluminescence (PL). The XRD patterns reveal well-developed reflections of hexagonal wurtzite ZnO without any indications of the phases related with Al or other impurities. The Raman results indicated the sharp peak located at 437 cm^{-1} indicates the typical wurtzite structure of ZnO and good crystallization. The PL spectra showed that the ZnO nanorods have two clear emission bands. For the two clear emission bands, one is a relatively weak and narrow UV emission centered about 380 nm that is widely accepted due to the exciton emission from conduction band to valence band and the other is much stronger and broader emission observed in the green-yellow range of visible spectrum with an emission peaks at 558 nm and 601 nm.

Introduction

Zinc oxide (ZnO) has been attracting particular interest because of its remarkable optical and electrical properties. Its significant optical transparency combined with an excellent electrical conductivity made ZnO as promising materials for fabrication of optoelectronic devices. ZnO is an n-type semiconductor with a wide direct band gap energy of 3.37 eV and along exciton binding energy of 60 meV at room temperature and has attracted more and more attention in the materials science because of the more expected applications in gas sensor [1] photocatalyst [2], solar cells [3-4], ultra violet light emitting materials [5], field effect transistors [6] and transparent conductors [7-9].

Recently, various chemical elements such as Al, Ga, Mn, Mg, and Co were doped into ZnO nanostructures due to the potential applications in spintronics and optoelectronic devices. It has been reported that the doping of Al can reach the highest conductivity without deterioration in optical transmission and crystallinity, and thus have been regarded as a potential alternative to the most accepted transparent conductive material, which is favorable for its applications in electronics, optoelectronics, and field emission devices [10-11]. Al doped ZnO nanostructures (nanowires, nanorods) have been prepared with various techniques, including electrochemical route [12-13], thermal oxidation [14], and hydrothermal process [15-17]. Among these synthesis methods, the hydrothermal process is

more facile and economic for the large scale fabrication of the nanostructures ZnO [18-19]. In addition Al doped ZnO nanostructures have attracted more and more attentions due to its low cost, nontoxic, and high transparent in visible region and especially the superior electrical conductivity. Most of the papers focused on the Al-doped ZnO nanograin thin films, whereas there are few reports on the nanostructure Al-doped ZnO with various morphologies.

In this paper, the synthesis of Al doped ZnO nanorods by a simple hydrothermal process have been carried out. Moreover, the influences of aluminum doping concentration on the micro-structural and optical characteristics of Al-doped ZnO nanorods have been investigated.

Experiment

Pure ZnO and Al-doped ZnO nanorods were grown on Si substrate by using seed-assisted hydrothermal method. The Si substrate (100) was cleaned using ultrasonic cleaning methods and rinsed in acetone for 15 min to remove pollutants from the surface of silicon substrate. The seed layer of ZnO films (100 nm) were first grown by RF magnetron puttering and in-situ annealing at 300 $^{\circ}$C for 1 hour. In a typical synthesis process, the substrate with ZnO seed layer was placed in an aqueous solution of 0.025M zinc nitrate hexahydrate ($Zn(NO_3)_2 \cdot 6H_2O$) appropriate amount of Aluminum nitrate $Al(NO_3)_3$ were dissolved by deionized water and 60 ml solution was received and 60 ml of sodium hydroxide

(NaOH) (5.0 mol/l) aqueous solution was slowly dripped into the former solution under magnetic stirring. In the solution, Al doping concentrations were chosen to 2at%, 4at%, 6at%, 8at%, and 10at%, respectively. Subsequently, the mixture was transferred into a 200 ml Teflon lined autoclave. Then the autoclave was sealed and maintained at 150 ˚C for 20 hours. After the reaction is complete, the precipitate is collected, washed with deionized water in the final products and finally dried at 100 ˚C for 5 hours.

The crystalline structure of the Al-doped ZnO samples was determined by X-ray diffraction (Cu K_α radiation, λ = 0.154056 nm). The morphology of as prepared un-doped and Al- doped ZnO sample were investigated by scanning electron microscopy (SEM). The optical property was characterized by Raman spectroscopy and Photoluminescence (PL).

Result and Discussion

The X-ray diffraction (XRD) was used to study the structure of ZnO nanorods. Figure 1 shows the X-ray diffraction patterns of the samples, which are prepared with the different Al-doped ZnO nanorods. The effects of different aluminum doped ZnO on the crystallographic structure are not revealed in Fig. 1. The XRD patterns reveal well-developed reflections of hexagonal wurtzite ZnO (JCPDS card No.036-1451), without any indications of the phases related with Al or other impurities

such as Al_2O_3, $ZnAl_2O_4$, NaOH etc. The lattice parameter of ZnO can be calculated by using Bragg's law.

According to Bragg's law $2d\sin\theta = n\lambda$, the lattice constant a and c of wurtzite structure ZnO were calculated by $\frac{1}{d_{hkl}^2} = \frac{4}{3}\left(\frac{h^2+hk+k^2}{a^2}\right) + \frac{l^2}{c^2}$. The lattice constant a was derived from $a = \frac{\lambda}{\sqrt{3}\sin\theta}$ for the (100) orientation and the lattice constant c was calculated as $c = \frac{\lambda}{\sin\theta}$ for the (002) orientation.

For pure ZnO nanorods, the lattice constant a was 0.3253 nm and c was 0.5207 nm. The values of lattice constants are nearly the standard of lattice constant of ZnO (a = 0.3249 nm and c = 0.5206 nm) [20]. This finding implies that the aluminum doping most probably occurs by substituting zinc atoms in the crystal structure. In comparison with the undoped sample by the increase in the intensity of ZnO peaks. The most intensive peak presented is shown as (101) plane and additional peaks along with (100) and (002) planes are also observed. The improvement of the crystallinity of ZnO nanorods with increasing Al doping contents is ascribed to the surface diffusion of the increasing adsorbed atoms, inducing an improvement of the quality and crystallinity. Although the absolute intensities of the peaks increased with the increasing of aluminum concentration, the intensities of these lines almost remained constant upon Al doping.

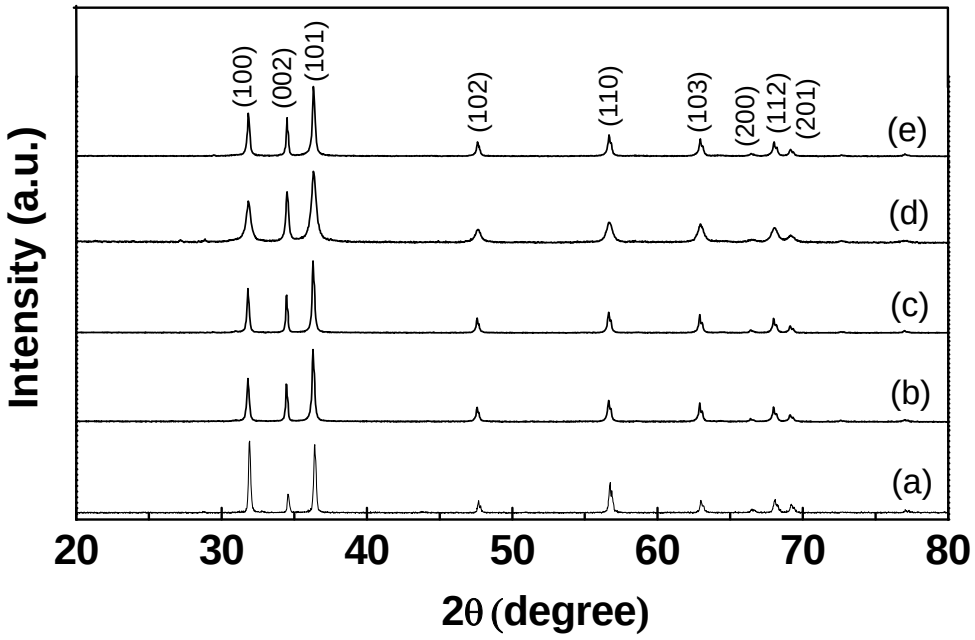

Figure 1: X-ray diffraction patterns of Al-doped ZnO nanorods: (a) ZnO, (b) 4at%Al, (c) 6at%Al, (d) 8at%Al, (e) 10at%Al.

The morphology of undoped and Al doped ZnO nanorods were investigated by field emission scanning electron microscopy (FE-SEM). Figure 2 shows the images of undoped and Al doped ZnO nanostructure grown by hydrothermal process. In this work, we found that undoped ZnO show small and short nanorods. At the same time, the nanorods are bundle together and consisted of other shapes. When the Al doped into ZnO ,the scanning electron microscope analysis for the samples synthesized under hydrothermal conditions shows the influence of the aluminum dopant contents on the nanorods morphology and length as shown in Fig. 2b – 2c. With the increasing aluminum content the morphology

changes from nanorods to nanosheet and particles. The network-like nanosheet can be found from Fig. 2(c). The product fabricated at the concentration of 8at%Al. To continue increasing the concentration of Al (10at%Al), the structure of ZnO tuned to be particle. This may be due to the Al doping institute the Zn and change the structure of ZnO.

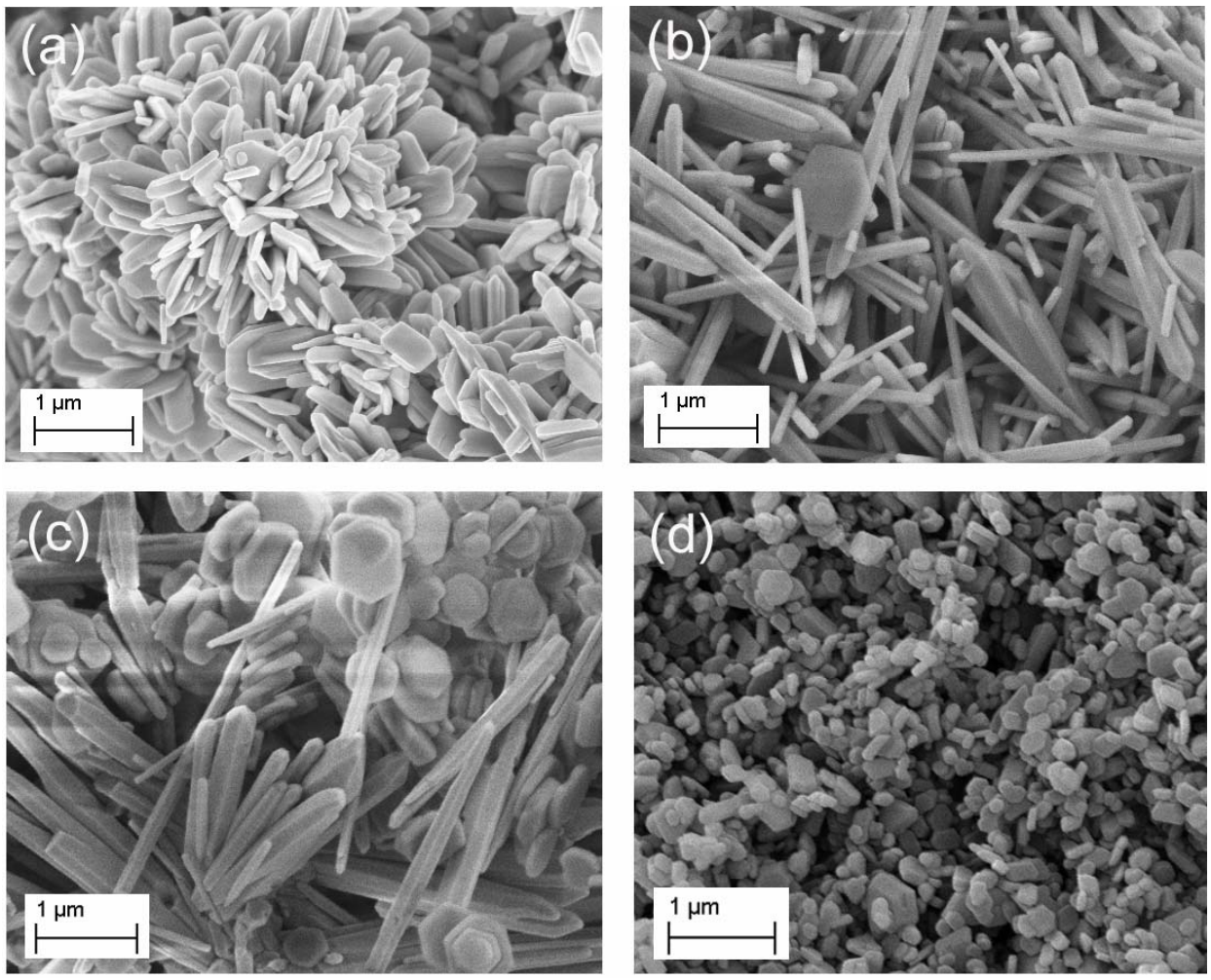

Figure 2: FESEM images of ZnO nanostructures with different concentration of Al-doped ZnO:

(a) ZnO, (b) 6at%Al, (c) 8at%Al, (d) 10at%Al.

The Raman-scattering spectra of the as grown ZnO structures are shown in Figure 3 with 514 nm laser green light as an excitation source. The Raman signals are usually very sensitive to the structure of crystal as well as to the defects in the crystal structure. The crystal structure of ZnO is wurtzite (hexagonal) which belongs to the C_{6v} symmetry group and gives the Raman-active optical phonon modes classified as A_1+ E_1+ $2E_2$ [21]. In addition, A1 and E1 modes are polar and split into transverse optical (TO) and longitudinal optical (LO) phonons. As a wide band gap oxides semiconductor, it is well known that ZnO has a strong optical absorption to the ultraviolet light (UV, e.g. 325 nm) and transparency to the visible light (e.g. 532 nm). Therefore, the UV Raman spectroscopy is more sensitive to the surface region of the sample, whereas the visible Raman spectroscopy gives not only the information of the surface but also the inner information of the sample [22].

Figure 3 gives the Raman spectra of the pure ZnO and Al doped ZnO nanostructures. The sharp peak located at 437 cm^{-1} corresponding to E2(high) mode indicates the typical wurtzite structure of ZnO and good crystallization. A transverse optical (TO) phonon mode was detected at 377 cm^{-1} (A1). The peaks at 328, 548, 724, 1052, 1065 and 1384 cm^{-1} are known to be multi-phonon responses [23-25]. In addition, the broad peak centered at 575 cm^{-1} assigned to A1(LO) mode is also detected. The peak intensity of E2 (high) mode, which is the characteristic peak of wurtzite ZnO, is found to be decreased with the increasing Al concentration. The intensities of peaks 1052 and 1065 cm^{-1} have been

obviously strengthened when the doping concentration of Al increased. It has been suggested that the mixing of two different cations by charge distribution and result in at least one vibration mode being strongly influenced. The additional peak at 724 cm^{-1} is associated with intrinsic lattice defects and often arises by doping with aluminum. However, these spectra clearly indicate that all the samples exhibit the well-known characteristics of the wurtzite structure of ZnO crystal. Therefore, the enhancement of surface-related phonon mode might be resulted from the doping of Al ions and/or the different morphology of ZnO nanostructures. The Al ions in ZnO host and different morphology of ZnO may change the electromagnetic interaction at the interfaces between the nanostructures.

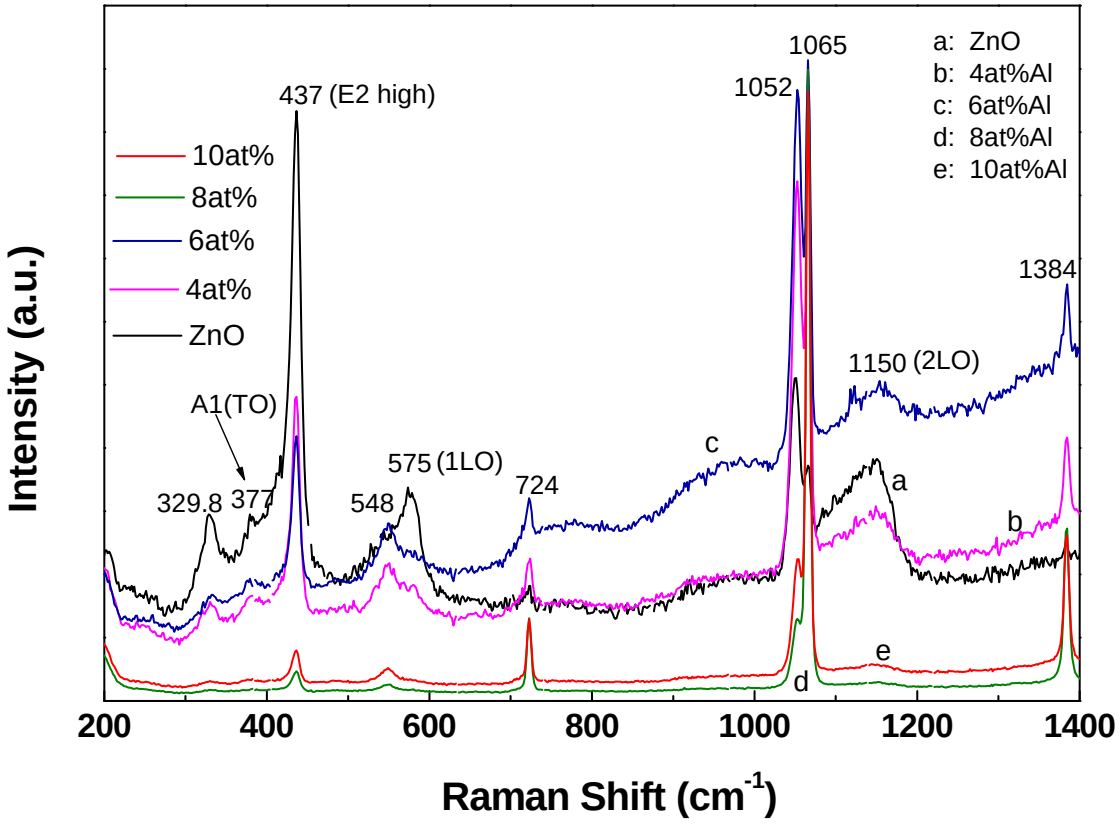

Figure 3: Room temperature Raman spectra of pure ZnO and Al doped ZnO nanorods. All the samples show qualitatively identical Raman shifts and they match well with the spectrum for wurtzite ZnO crystal.

The photoluminescence measurement of ZnO nanorods were performed with an excitation wavelength 325 nm at room temperature. Figure 4 shows the PL spectra of ZnO nanorods at room temperature growth by hydrothermal technique with various Al doping concentrations. The PL spectra for pure ZnO showed a weak and narrow UV emission band around 378 nm. In addition, a much

stronger and broader emission band is located in the green-yellow part of the visible spectrum with an emission peaks at 560 nm and 602 nm, respectively.

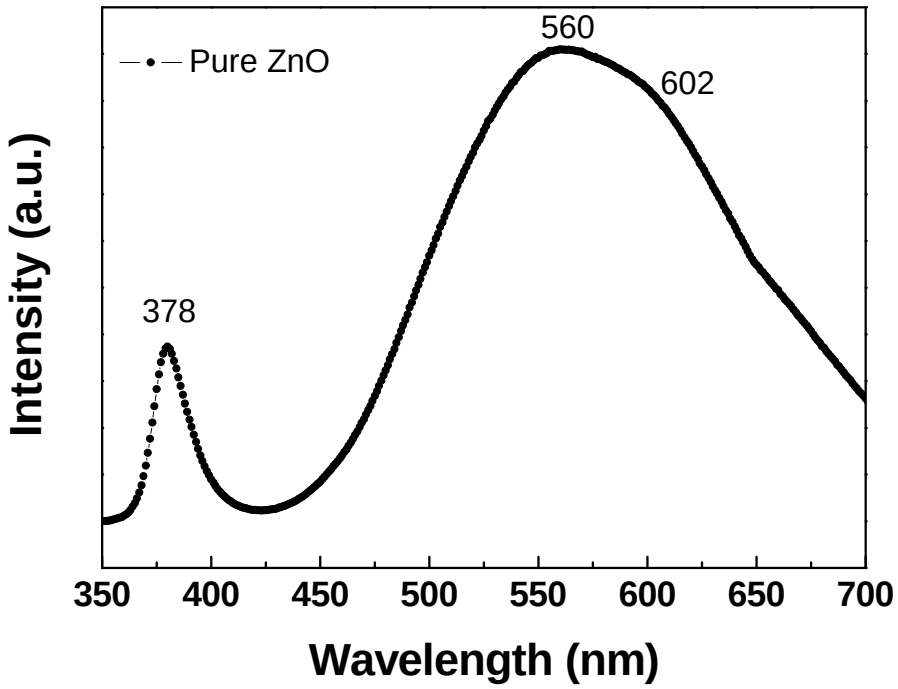

Figure 4: PL spectra of pure ZnO nanorods using 325 nm lines as the exciting source.

As we know, the origin of the near-UV luminescence is attributed to the excited electron emitted from the conduction band to valence band [26] Therefore, the peak at 378 nm is due to the exciton emission from conduction band to valence band, which is an intrinsic property of ZnO. Moreover, it is reasonable to assume that the visible luminescence at 560 nm and 602 nm in this study occurs primarily resulted from the intrinsic or extrinsic defects. The intrinsic defects are associated with deep

level emissions such as oxygen vacancies, zinc interstitials, zinc vacancies, oxygen interstitials, or oxygen anti-sites [27]. Moreover, the extrinsic defects are likely to have resulted from absorbed water or surface hydroxyl groups [28–30].

From Figure 5, the PL results of Al doped ZnO nanorods showed two clear emission bands. One is a relatively weak and narrow UV emission centered about 380 nm that is widely accepted due to the exciton emission from conduction band to valence band and the other is much stronger and broader emission observed in the green-yellow range of visible spectrum with an emission peak around 558 nm and 601 nm that is believed to be caused by extrinsic impurities such as absorbed water or surface hydroxyl groups. The strong UV emission, which strongly relate to crystallite quality of ZnO, is contribute by conduction valence band combination (∼ 375 nm). It is shallow donor (∼ 395 nm) and Zn interstitial (∼ 420 nm) [31-33].

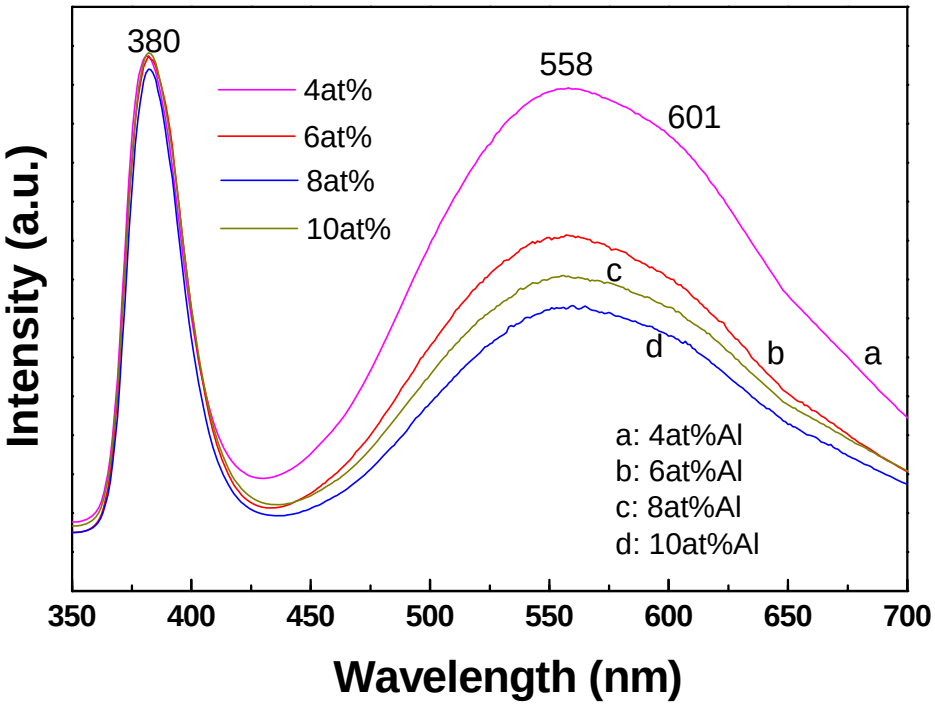

Figure 5: PL spectra of Al doped ZnO nanorods using 325 nm lines as the exciting source.

Conclusion

In conclusion, Al-doped zinc oxide nanorods were successfully grown on a silicon substrate using a hydrothermal process. The effect of Al doping on the elemental composition, microstructure characteristics and optical properties of the nanorod arrays has been studied. XRD patterns illustrate that the nanorods were ZnO wurtzite structure. The Raman results indicated the sharp peak located at 437 cm^{-1} corresponding to E2(high) mode indicates the typical wurtzite structure of ZnO and good

crystallization and the broad peak centered at 575 cm^{-1} assigned to A1(LO) mode is also detected. The PL spectra showed that the ZnO nanorods have two clear emission bands. For the two clear emission bands, one is a relatively weak and narrow UV emission centered about 380 nm that is widely accepted due to the exciton emission from conduction band to valence band and the other is much stronger and broader emission observed in the green-yellow range of visible spectrum with an emission peaks at 558 nm and 601 nm that is believed to be caused by extrinsic impurities such as absorbed water or surface hydroxyl groups.

Acknowledgment

This work was supported by the funds from Thailand Research Fund (Grant No. MRG5480254).

References

1. T. Gao, T.H. Wang, Appl. Phys. A 80 (2005) 1451.

2. S. Anandan, A. Vinu, T. Mori, N. Gokulakrishnan, P. Srinivasu, V. Murugesan, K. Ariga, Catal. Commun. 8 (2007) 1377.

3. X.L. Chen, B.H. Xu, J.M. Xue, Y. Zhao, C.C. Wei, J. Sun, Y. Wang, X.D. Zhang, X.H. Geng, Thin Solid Films 515 (2007) 3753.

4. H. Chen, A.D. Pasquier, G. Saraf, J. Zhong, Y. Lu, Semicond. Sci. Technol. 23 (2008) 045004.

5. Y.R. Ryu, J.A. Lubguban, T.S. Lee, H.W. White, T.S. Jeong, C.J. Youn, B.J. Kim, Appl. Phys. Lett. 90 (2007) 131115.

6. Z.X. Xu, V.A.L. Roy, P. Stalling, M. Muccini, S. Toffanin, H.F. Xiang, C.M. Che, Appl. Phys. Lett. 90 (2007) 223509.

7. I. Kim, K.S. Lee, T.S. Lee, J.H. Jeong, B.K. Cheong, Y.J. Baik, W.M. Kim, J. Appl. Phys. 100 (2006) 063701.

8. K.M. Lin, P. Tsai, Thin Solid Films 515 (2007) 8601.

9. M. Lv, X. Xiu, Z. Pang, Y. Dai, L. Ye, C. Cheng, S. Han, Thin Solid Films 16 (2008) 2017.

10. S.N. Yun, J.Y. Lee, J.Y. Yang, S.W. Lim, Physica B:Condensed Matter 405 (2010) 413.

11. R.C. Wang,C.P. Liu, J.L. Huang, S.J.Chen, Applied Physics Letters 88 (2006).

12. J. Cui, U.J. Gibson, J. Phys. Chem. B 109 (2005) 22074.

13. G.R. Li, X.H. Lu, W.X. Zhao, C.Y. Su, Y.X. Tong, Cryst. Growth Des. 8 (4) (2008) 1276.

14. L.C. Chao, J.W. Lee, C.C. Liau, J. Phys. D: Appl. Phys. 41 (2008) 115405.

15. H.Q. Wang, G.Z. Wang, L.C. Jia, C.J. Tang, G.H. Li, J. Phys. D: Appl. Phys. 40 (2007) 6549.

16. T. Ma, M. Guo, M. Zhang, Y. Zhang, X. Wang, Nanotechnology 18 (2007) 035605.

17. J. Song, S. Lim, J. Phys. Chem. C 111 (2007) 596.

18. C. Yan, D. Xue, J. Alloy. Compd. 431 (2007) 241.

19. C. Yan, D. Xue, J. Phys. Chem. B 110 (2006) 1581.

20. L. Oleg, C. Lee, K.O. luis, R.C. Beatriz, C. Guangyu, K. Hani, P. Sanghoon and S. Alfons, J Phys. Chem. C 144 (2010) 12401.

21. Y. Tong, Y. Liu, C. Shao, Y. Liu, C. Xu, J. Zhang, Y. Lu, D. Shen, X. Fan, J. Phys. Chem. B 110 (2006) 14714.

22. M. Li, Z. Feng, G. Xiong, P. Ying, Qin Xin, Can Li, J. Phys. Chem. B 105 (2001) 8107.

23. T. C. Damen, S. P. S. Porto and B. Tell, Phys. Rev. 142 (1966) 570.

24. C. Bundesmann, N. Ashkenov, M. Schubert, D. Spemann, T. Butz, E. M. Kaidashev, M. Lorenz and M Grundmann, Appl. Phys. Lett. 83 (2003) 1074.

25. W. Gebicki, K. Osuch, C. Jastrezebski, Z. Golacki and M. Godlewski, Superlattices Microstruct. 38, (2005) 428.

26. D.C. Reynolds, D.C. Look, B. Jogai, J.E. Hoelscher, R.E. Sherriff, M.T. Harris, M.J. Callahan, J. Appl. Phys. 88 (2000) 2152.

27. Y.P. Wang, W.I. Lee, T.Y. Tseng, Appl. Phys. Lett. 69 (1996) 1807.

28. R. Xie, D. Li, D. Yang, T. Sekiguchi, M. Jiang, Nanotechnology 17 (2006) 2789.

29. K.H. Tam, C.K. Cheung, Y.H. Leung, A.B. Djurisic, C.C. Ling, C.D. Beling, S. Fung,W.M. Kwok,W.K. Chan, D.L. Phillips, L. Ding,W.K. Ge, J. Phys. Chem., B 110 (2006) 20865.

30. N.S. Norberg, D.R. Gamelin, J. Phys. Chem., B 109 (2005) 20810.

31. M.W. Ahn, K.S. Park, J.H. Heo, J.G. Park, D.W. Kim, K.J. Choi, J.H. Lee, S.H. Hong, Applied Physics Letters **93**, (2008) 263103(1) - 263103(3).

32. L.M. Li, Z.F. Du, T.H. Wang, Sensors and Actuators B: Chemical **147** (2010) 165.

33. N. Han, X. Wu, L. Chai, H. Liu, Y. Chen, Sensors andActuators B: Chemical **150** (2010) 230.

Output

The out put in this work is the prototype that can be used to sense the ethanol and CO gas. We have been successful to fabricate the ZnO nanostructure and also testing gas even though the result of response of CO gas is not good enough but we can use this result to improve the samples in the future.

In addition, we have submitted the manuscript to Journal of alloys and compounds. Now the situation of the paper is under review and we also plane to submit another paper about sensor and we are waiting for the new results that we are doing. In the future, we can make the completely prototype by using our sample.